Physics of Plasmas ARTICLE scitation.org/journal/php

Verification of a fully kinetic ion model for electromagnetic simulations of high-frequency waves in toroidal geometry

Cite as: Phys. Plasmas **29**, 073902 (2022); doi: 10.1063/5.0090168
Submitted: 3 March 2022 · Accepted: 23 June 2022 ·
Published Online: 13 July 2022

Y. Y. Yu,[1,2] X. S. Wei,[2] P. F. Liu,[2] and Z. Lin[2,a)]

AFFILIATIONS

[1]Fusion Simulation Center, Peking University, Beijing 100871, China
[2]Department of Physics and Astronomy, University of California, Irvine, California 92697, USA

[a)]Author to whom correspondence should be addressed: zhihongl@uci.edu

ABSTRACT

For the study of high-frequency electromagnetic waves in tokamaks, an electromagnetic simulation model, in which the ion dynamics is described by a six-dimensional Vlasov equation and the electron dynamics is described by a drift kinetic equation, is formulated and implemented in the global gyrokinetic toroidal code (GTC). Analytic dispersion relations are derived in reduced systems and compared with various theories to verify the model. Linear simulations of a generalized ion Bernstein wave and ion cyclotron emission are verified by comparing the GTC simulation results with analytic dispersion relation theory and magnetoacoustic cyclotron instability theory, respectively, in cylindrical geometry.

I. INTRODUTION

There are a variety of high-frequency waves excited by energetic particles in fusion plasmas, such as compression Alfvén eigenmodes (CAE), global Alfvén eigenmodes (GAE), and ion cyclotron emission (ICE), recently observed in many tokamaks.[1–10] Many new phenomena arising from high-frequency modes need more experimental, theoretical, and simulation research to understand their effects on plasma confinement and their potential roles as diagnostic tools for α-particles in burning plasmas.

CAEs and GAEs typically have a frequency close to the ion gyrofrequency. They can be driven by super- Alfvénic energetic particles and are frequently observed in the NSTX-U and DIII-D tokamak experiments with low magnetic fields. The 3D hybrid MHD-kinetic code HYM,[11] in which fast ions are simulated using the particle-in-cell (PIC) method and full-orbit equations of motion, has been used in simulations of CAE and GAE excitation and stabilization in the NSTX-U.[12,13] ICEs, on the other hand, are usually excited due to magnetoacoustic cyclotron instability (MCI), in which the compression Alfvén wave frequency is close to the harmonics of the energetic ion gyrofrequency. The basis for diagnostic exploitation of the ICE has been greatly strengthened by recent nonlinear simulations using fully kinetic ions and fluid electrons in a slab geometry.[14] Such simulations have confirmed that ICE intensity scales linearly with concentration of energetic ions (n_f/n_0, where n_f is the energetic ion density and n_0 is the electron density), which agrees with the measurement in the JET tokamak.[15–17] Therefore, ICE potentially offers a unique diagnostic tool for the α-particles produced by a fusion reaction and is planned to be used in future deuterium-tritium experiments in the ITER tokamak.[18] These local simulations of the ICE in a simplified geometry, however, cannot address some key physics, such as mode structure, the time evolution, and the dependence on the fast-ion distributions, as observed in the DIII-D experiments.[9]

To simulate high-frequency waves whose frequency is close to or higher than the ion cyclotron frequency, a fully kinetic ion model is needed to resolve the ion cyclotron motion. An electromagnetic, fully kinetic, PIC simulation model has been used in EPOCH[19] and iPIC3D[20] simulations of the ICE[21] and magnetic reconnection,[20] respectively, using Cartesian coordinates for slab geometry. In space plasma simulations, there are also several electromagnetic models in which ions are fully kinetic, such as GeFi[22] and AIKEF.[23] In tokamak plasma simulations, however, accurate description of the toroidal geometry is essential for the study of resonant excitation and mode structures, which is absent in the models mentioned above. The kinetic-MHD toroidal codes HYM and M3D-K[24] use an MHD model for thermal plasmas and a gyrokinetic model for energetic particles to describe the macroscopic behavior of plasmas, although the kinetic effects of thermal plasmas can in principle be incorporated. In previous gyrokinetic toroidal code (GTC)[25] simulations, the Boris push has been implemented for integrating the full particle orbit in cylindrical[26] and toroidal geometries.[27] In the electrostatic simulation using fully kinetic ions, a linear

dispersion relation and nonlinear particle trapping have been verified for a lower hybrid wave (LHW)[28] and an electrostatic ion Bernstein wave (IBW).[29] The frequency and mode structure in simulations agree well with those of theoretical prediction.[30] GTC simulations using fluid ions and drift kinetic electrons have also been carried to study the LHW linear mode conversion and absorption in the toroidal geometry.[31]

In this work, we extend the GTC simulation in the toroidal geometry to the electromagnetic simulation model, in which the ion dynamics is described by a six-dimensional Vlasov equation and the electron dynamics is described by a drift kinetic equation. An analytical dispersion relation is derived in two reduced systems with massless fluid electrons. We implement the model in the GTC code and carry out linear simulations of waves propagating in the perpendicular (to an equilibrium magnetic field) direction, in which the electron response can be neglected. In these simulations, the compressional Alfvén wave and the generalized IBW[32] frequency are verified using an analytical dispersion relation. Then, simulations of both thermal and energetic ions are carried out for the ICE excitation. Consistent with analytic theory,[33] GTC simulation results show that the ICE linear growth rate is approximately proportional to the square-root of the concentration of the energetic ions (n_f/n_0), and that different cyclotron harmonics have comparable growth rates.

The remainder of this paper is organized as follows. Section II describes the formulation of the kinetic simulation model for high-frequency waves in toroidal geometry. The analytic dispersion relations in reduced systems are derived and compared with a fully kinetic model in Sec. III. The verification of GTC simulations of the generalized IBW dispersion relation and the excitation of ICE is presented in Sec. IV. Finally, Sec. V presents the conclusion and discussion.

II. SIMULATION MODEL

To study high-frequency electromagnetic waves in a tokamak, we develop a new electromagnetic simulation model with fully kinetic ions and drift kinetic electrons. In Sec. II A, we use a Vlasov equation in six-dimensional phase space to describe the ion dynamics. In Sec. II B, we employ a drift kinetic equation to describe the electron dynamics. Then, field equations, including Poisson's equation, the parallel Ampère's law, and the electron perpendicular force balance equation are used to close the system in Sec. II C.

A. Fully kinetic ions

For fully kinetic ions, the dynamics is governed by a Vlasov equation in six-dimensional phase space:

$$Lf_i(\mathbf{r},\mathbf{v},t)=0. \tag{1}$$

Here $\mathbf{r}$, $\mathbf{v}$, t are the particle position, velocity, and time, respectively; f_i is an ion distribution function; and L is a nonlinear propagator, which can be decomposed into an equilibrium part L_0 and a perturbed part δL, $L=L_0+\delta L$:

$$L_0=\frac{\partial}{\partial t}+\mathbf{v}\cdot\nabla+\frac{q_i}{m_i c}\mathbf{v}\times\mathbf{B_0}\cdot\nabla_{\mathbf{v}}, \tag{2}$$

$$\delta L=\frac{q_i}{m_i}\left(\boldsymbol{\delta}\mathbf{E}+\frac{1}{c}\mathbf{v}\times\boldsymbol{\delta}\mathbf{B}\right)\cdot\nabla_{\boldsymbol{v}}, \tag{3}$$

where q_i and m_i are the ion charge and ion mass, $\mathbf{B_0}$ is the equilibrium magnetic field, and $\boldsymbol{\delta}\mathbf{E}$ and $\boldsymbol{\delta}\mathbf{B}$ are the perturbed electric field and perturbed magnetic field, respectively. The ion distribution function is also decomposed into an equilibrium part and perturbed part as $f=f_{i0}+\delta f_i$. The equilibrium distribution f_{i0} obeys

$$L_0 f_{i0}=0. \tag{4}$$

The solution of this equation is any distribution function of constants of motion, e.g., uniform isotropic Maxwellian and modified slowing down distribution used in this work. Defining the particle weight as $w_i=\delta f_i/f_i$, we obtain the weight evolution equation:

$$\frac{dw_i}{dt}=-\frac{1-w_i}{f_{i0}}\delta L f_{i0}. \tag{5}$$

The ion motion in the phase space under self-consistent electromagnetic fields is given by

$$\frac{d\mathbf{v}}{dt}=\frac{q_i}{m_i}\left(\delta\mathbf{E}+\frac{1}{c}\mathbf{v}\times\mathbf{B}\right), \tag{6}$$

$$\frac{d\mathbf{r}}{dt}=\mathbf{v}. \tag{7}$$

We use the Boris scheme in magnetic coordinates to push ions in the GTC code.[27] The perturbed number density δn_i and current density $\delta\mathbf{j_i}$ can be obtained from the velocity moments of δf_i, i.e.,

$$\delta n_i=\int\delta f_i d\mathbf{v}, \tag{8}$$

$$\delta\mathbf{j_i}=\mathrm{q}_i\int\mathbf{v}\delta f_i d\mathbf{v}. \tag{9}$$

Here, the particle charge and current are deposited onto the surrounding eight grid points in the 3D space using linear interpolation.[34]

B. Drift kinetic electrons

The electrons are described by the drift kinetic equations.[35] Using the gyrocenter position $\mathbf{X}$, parallel velocity $v_{||}$, and magnetic moment μ as independent variables in five-dimensional phase space, the drift kinetic equation is

$$L_g f_e(\mathbf{X},v_{||},\mu,t)=0, \tag{10}$$

where f_e is the electron distribution function and L_g is the gyrocenter propagator in symplectic form.[35] L_g can be decomposed into an equilibrium part L_{g0}, a first-order linear part δL_{g1}, and a second-order nonlinear part δL_{g2} as $L_{g0}+\delta L_{g1}+\delta L_{g2}$:

$$L_{g0}=\frac{\partial}{\partial t}+\left(\frac{v_{||}}{B_0}\mathbf{B_0^*}+\frac{c\mathbf{b_0}}{q_e B_0}\times\mu\nabla B_0\right)\cdot\nabla-\frac{\mu}{m_e B_0}\mathbf{B_0^*}\cdot\nabla B_0\frac{\partial}{\partial v_{||}}, \tag{11}$$

$$\delta L_{g1}=\left(v_{||}\frac{\boldsymbol{\delta}\mathbf{B}_\perp}{B_0}+\frac{c\mathbf{b_0}}{q_e B_0}\times\left(q_e\nabla\delta\phi+\mu\nabla\delta B_{||}\right)\right)\cdot\nabla+\left(-\frac{\mu}{m_e B_0}\boldsymbol{\delta}\mathbf{B}_\perp\cdot\nabla B_0-\frac{\mathbf{B_0^*}}{m_e B_0}\cdot\left(q_e\nabla\delta\phi+\mu\nabla\delta B_{||}\right)-\frac{q_e}{cm_e}\frac{\partial\delta A_{||}}{\partial t}\right)\frac{\partial}{\partial v_{||}}, \tag{12}$$

$$\delta L_{g2}=-\frac{\boldsymbol{\delta}\mathbf{B}_\perp}{m_e B_0}\cdot\left(q_e\nabla\delta\phi+\mu\nabla\delta B_{||}\right)\frac{\partial}{\partial v_{||}}, \tag{13}$$

where $\mathbf{B}^* = \mathbf{B}_0^* + \boldsymbol{\delta}\mathbf{B}_\perp$, $\mathbf{B}_0^* = \mathbf{B}_0 + \frac{B_0 v_{||}}{\Omega_e}\nabla \times \mathbf{b}_0$, and $\boldsymbol{\delta}\mathbf{B}_\perp = \nabla_\perp \times (\delta A_{||}\mathbf{b}_0)$. $\mathbf{B}_0 = B_0\mathbf{b}_0$ is the equilibrium magnetic field; Ω_e is the electron cyclotron frequency; q_e and m_e are the electron charge and electron mass, respectively; and $\delta\phi$, $\delta B_{||}$, and $\delta A_{||}$ are the perturbed electrostatic potential, perturbed parallel magnetic field, and parallel vector potential, respectively. Then, the distribution function is decomposed into an equilibrium part and a perturbed part as $f_e = f_{e0} + \delta f_e$. The equilibrium distribution f_{e0} satisfies

$$L_{g0} f_{e0} = 0. \tag{14}$$

f_{e0} is approximated as a Maxwellian distribution function by neglecting electron finite Larmor radius effects and equilibrium parallel flow, assuming the effects of the equilibrium current are not important for the high-frequency modes such as ICE: $f_{e0} = n_0\left(\frac{m_e}{2\pi T_{e0}}\right)^{3/2}\exp\left(-\frac{m_e v_{||}^2 + 2\mu B_0}{2T_{e0}}\right)$. n_0 and T_{e0} are the equilibrium electron density and electron temperature, respectively. From Eqs. (10) and (14), we have

$$L_{g0}\delta f_e + \delta L_{g1} f_{e0} + \delta L_{g1}\delta f_e + \delta L_{g2} f_{e0} + \delta L_{g2}\delta f_e = 0. \tag{15}$$

Defining weight as $w_e = \delta f_e / f_e$, the weight evolution equation can be written as

$$\frac{dw_e}{dt} = L_g w_e = -\frac{(1-w_e)}{f_{e0}}\left(\delta L_{g1} + \delta L_{g2}\right) f_{e0}. \tag{16}$$

The equations of particle motion corresponding to Eq. (10) are given in Appendix A of Bao's paper.[35]

We keep only the leading linear and nonlinear terms based on the ordering: $u_{||e0} = \frac{1}{n_0}\int v_{||} f_{e0} d\boldsymbol{v} \approx 0$, $k_{||} \ll k_\perp$, $k_\perp c/\omega_{pe} \sim 1$, $\delta n_e/n_0 \sim \delta P_{||e}/P_{||e} \sim \delta B_{||}/B_0 \sim \delta B_\perp/B_0$, $\nabla n_0/n_0 \sim \nabla T_{e0}/T_{e0} \sim 1/a_{minor}$, $\nabla B_0/B_0 \sim 1/R$, $a/R < 1$. Here, ω_{pe} is the electron plasma frequency; $k_{||}$ and $k_\perp$ are the absolute values of the parallel and perpendicular wave vectors, respectively; and a and R are the tokamak minor radius and major radius, respectively. We then integrate Eq. (15) in the gyrocenter velocity space to derive the electron continuity equation:

$$\begin{aligned}
&\frac{\partial \delta n_e}{\partial t} + \mathbf{B}_0\cdot\nabla\left(\frac{n_0\delta u_{e||}}{B_0}\right) + B_0\mathbf{v}_\mathbf{E}\cdot\nabla\left(\frac{n_0}{B_0}\right) \\
&\quad - n_0(\mathbf{v}^* + \mathbf{v}_\mathbf{E})\cdot\frac{\nabla B_0}{B_0} + \frac{c\mathbf{b}_0\times\nabla\delta B_{||}}{B_0^2}\cdot\frac{\nabla P_{\perp e0}}{q_e} \\
&\quad + \boldsymbol{\delta}\mathbf{B}_\perp\cdot\nabla\left(\frac{n_0\delta u_{e||}}{B_0}\right) + B_0\mathbf{v}_\mathbf{E}\cdot\nabla\left(\frac{\delta n_e}{B_0}\right) \\
&\quad + \frac{c\mathbf{b}_0\times\nabla\delta B_{||}}{B_0^2}\cdot\frac{\nabla\delta P_{\perp e}}{q_e} = 0,
\end{aligned} \tag{17}$$

where $\delta u_{e||} = \frac{1}{n_0}\int v_{||}\delta f_e d\mathbf{v}$ is the perturbed parallel velocity; $\delta P_{||e} = m_e\int v_{||}^2\delta f_e d\mathbf{v}$ and $\delta P_{\perp e} = \int \delta f_e \mu B_0 d\mathbf{v}$ are the perturbed parallel and perpendicular pressures, respectively; $P_{\perp e0} = \int \mu B_0 f_{e0} d\mathbf{v} = n_0 T_{e0}$ is the equilibrium perpendicular pressure; $\mathbf{v}_\mathbf{E} = \frac{c\mathbf{b}_0\times\nabla\phi}{B_0}$ is the $\mathbf{E}\times\mathbf{B}$ drift velocity; $\boldsymbol{v}^* = \frac{\mathbf{b}_0\times\nabla\left(\delta P_{\perp e} + \delta P_{||e}\right)}{n_0 m_e\Omega_e}$ is the perturbed diamagnetic drift velocity; and $\int d\mathbf{v} = \frac{2\pi B_0}{m_e}\int dv_{||}d\mu$. Equation (17) is solved on the spatial grids using finite difference method for perturbed quantities and B-spline interpolation for equilibrium quantities.[34] Similarly, we integrate Eq. (15) based on the same ordering to obtain the parallel momentum equation:

$$\begin{aligned}
&n_0\frac{\partial\delta u_{e||}}{\partial t} + \frac{q_e n_0}{m_e}\mathbf{b}_\mathbf{0}\cdot\nabla\delta\phi + \frac{q_e n_0}{m_e c}\frac{\partial\delta A_{||}}{\partial t} + \frac{B_0}{m_e}\mathbf{b}_\mathbf{0}\cdot\nabla\left(\frac{\delta P_{||e}}{B_0}\right) \\
&\quad + \frac{\mathbf{B}_\mathbf{0}\cdot\nabla\delta B_{||}}{m_e B_0^2}P_{\perp e0} + \frac{q_e\delta n_e}{m_e}\mathbf{b}_\mathbf{0}\cdot\nabla\delta\phi + \frac{q_e\delta n_e}{m_e c}\frac{\partial\delta A_{||}}{\partial t} \\
&\quad + \frac{q_e n_0}{m_e B_0}\boldsymbol{\delta}\mathbf{B}_\perp\cdot\nabla\delta\phi + \frac{\boldsymbol{\delta}\mathbf{B}_\perp}{m_e}\cdot\nabla\left(\frac{\delta P_{||e}}{B_0}\right) + B_0\mathbf{v}_\mathbf{E}\cdot\nabla\left(\frac{n_0\delta u_{e||}}{B_0}\right) = 0.
\end{aligned} \tag{18}$$

C. Field equations

In the particle simulation, the plasma is treated as a set of computational particles interacting with each other through self-generated electromagnetic fields. To close the system, therefore, we need to solve the field equations. The electrostatic is solved by the Poisson's equation for fully kinetic ions and drift kinetic electrons:[35]

$$\begin{aligned}
&\left(1 + \frac{\omega_{pe}^2}{\Omega_e^2}\right)\nabla_\perp^2\delta\phi - \frac{\omega_{pe}^2}{\Omega_e^2}\frac{\omega_{pe}^2}{c^2}\frac{\delta\phi}{1+0.5\beta_e} \\
&\quad = -4\pi\left(q_i\delta n_i + q_e\delta n_e - q_e\frac{\beta_e}{2+\beta_e}\frac{\delta P_{\perp e}}{T_e}\right) - \frac{\omega_{pe}^2}{\Omega_e^2}\frac{\omega_{pe}^2}{c^2}\frac{\chi}{1+0.5\beta_e},
\end{aligned} \tag{19}$$

where $\beta_e = 8\pi n_0 T_e/B_0{}^2$. The parallel vector potential is solved by the parallel Ampère's law ($k_{||} \ll k_\perp$):

$$\nabla_\perp^2\delta A_{||} = -\frac{4\pi}{c}\left(j_{i||} + q_e n_0\delta u_{e||}\right). \tag{20}$$

Finally, the compressible magnetic perturbation is solved from the perpendicular electron force balance equation,[35]

$$\delta B_{||} = \frac{4\pi}{B_0(1+0.5\beta_e)}\left(n_0 q_e\chi - n_0 q_e\delta\phi - \delta P_{\perp e}\right). \tag{21}$$

Here, the effective potential χ for the perturbed Lorentz force is defined[35] as

$$\nabla_\perp^2\chi = -\frac{1}{n_0 q_e c}\nabla_\perp\cdot\left(\boldsymbol{\delta}\mathbf{j}_{i\perp}\times\mathbf{B}_0\right). \tag{22}$$

The perturbed electric field is defined by the perturbed scalar and vectors potential:

$$\nabla_\perp^2\mathbf{A}_\perp = -\nabla\delta B_{||}\times\hat{\mathbf{b}}_0, \tag{23}$$

$$\boldsymbol{\delta}\mathbf{E} = -\nabla\delta\phi - \frac{1}{c}\frac{\partial\boldsymbol{\delta}\mathbf{A}}{\partial t}. \tag{24}$$

Now, we complete the formulation of the fully kinetic ion model for electromagnetic simulations. These field equations are solved by GTC in a field-aligned mesh[36] using either finite difference method[34] or the finite element method.[37]

III. ANALYTIC DISPERSION RELATION IN REDUCED SYSTEMS

In order to verify the simulation model given in Sec. II, we derive a corresponding linear dispersion for two reduced systems. Here, we

consider uniform ambient magnetic field and uniform equilibrium plasma density and temperature profiles. Furthermore, we reduce the drift kinetic electrons to massless cold fluid electrons, retaining only the linear terms. Then, Eqs. (17), (18), and (21) reduce, respectively, to

$$\frac{\partial \delta n_e}{\partial t} = -n_0 \hat{\mathbf{b}}_\mathbf{0} \cdot \nabla \delta u_{e||}, \tag{25}$$

$$\frac{\partial \delta A_{||}}{\partial t} = -c\hat{\mathbf{b}}_\mathbf{0} \cdot \nabla \delta \phi, \tag{26}$$

$$\delta B_{||} = \frac{4\pi n_0 q_e}{B_0}(\chi - \delta\phi). \tag{27}$$

Using the quasi-neutrality condition, Poisson's equation [Eq. (19)] reduces to

$$\delta\phi = \frac{B_0^2}{4\pi n_0^2 q_e^2}(q_i \delta n_i + q_e \delta n_e) + \chi. \tag{28}$$

Since electrons move much faster than ions in the parallel direction, we can neglect the perturbed parallel ion current. Then, from the parallel Ampère's law, we have

$$\delta u_{e||} = \frac{c}{4\pi e n_0}\nabla_\perp^2 \delta A_{||}. \tag{29}$$

A. Two fluid, cold plasmas

In the first reduced system, we treat ions as cold fluid plasmas and $q_i = -q_e = e$. The ion continuity equation is

$$\frac{\partial \delta n_i}{\partial t} + n_0 \nabla_\perp \cdot \delta \mathbf{u}_{\mathbf{i}\perp} = 0. \tag{30}$$

Using the ion dynamic equation and normal mode ansatz, $\frac{\partial}{\partial t} = -i\omega$, $\nabla = \mathrm{i}\mathbf{k}$, we easily derive the following equation:

$$\delta \mathbf{u}_{\mathbf{i}\perp} = \frac{i\omega q_i}{m_i\left(\omega^2 - \Omega_i^2\right)}\left(\delta \mathbf{E}_\perp + \frac{i\Omega_i}{\omega}\delta \mathbf{E}_\perp \times \hat{\mathbf{b}}_\mathbf{0}\right). \tag{31}$$

Combining the definition of perpendicular ion current,

$$\delta \mathbf{j}_{\mathbf{i}\perp} = n_0 q_i \delta \mathbf{u}_{\mathbf{i}\perp}, \tag{32}$$

together with Eqs. (22)–(31), and using the non-trivial solution condition, we derive the dispersion relation as

$$\left(S' - n_{||}{}^2\right)\left(S' - n_\perp{}^2\right) - D'^2 = 0, \tag{33}$$

where

$$S' = \frac{\omega_{pi}{}^2}{\Omega_i{}^2}\frac{1}{1 - (\omega/\Omega_i)^2} \approx S - 1, \tag{34}$$

$$D' = -\frac{\omega_{pe}{}^2}{\omega\Omega_e} + \frac{\omega_{pi}{}^2\Omega_i}{\omega\left(\omega^2 - \Omega_i^2\right)} \approx D. \tag{35}$$

S and D have the same definitions as those in Stix's cold fluid theory:[38]

$$L = 1 - \sum_s \frac{\omega_{\mathrm{ps}}{}^2}{\omega(\omega - \Omega_s)},$$

$$R = 1 - \sum_s \frac{\omega_{\mathrm{ps}}{}^2}{\omega(\omega + \Omega_s)},$$

$$S = \frac{1}{2}(R + L),$$

$$D = \frac{1}{2}(R - L).$$

The difference between S' and S comes from the fact that we have dropped the displacement current in our model. In Eq. (33), the factor $S' - n_\perp{}^2$ corresponds to $\mathrm{S} - n^2$ in the ideal MHD theory. The difference comes from the fact that we assume $k_{||} \ll k_\perp$ in the parallel Ampère's law and the perpendicular force balance equation, and we also drop some coupling terms between the parallel and perpendicular wave vectors.

When we derive the parallel dispersion relation, therefore, we use the assumption $n_\perp \gg n_{||}$ instead of letting $n_\perp = 0$,

$$\frac{D^2}{n_\perp^2 - S} = \frac{y^2 S^2}{n_\perp^2 - S} \sim \frac{y^2 n_{||}^2}{n_\perp^2} \sim 0,$$

where $y = \frac{\omega}{\Omega_i}$. Furthermore, we have

$$k_{||}^2 v_A^2/\Omega_i^2 = y^2/\left(1 - y^2\right), \tag{36}$$

which is the dispersion relation of a shear Alfvén wave modified by an ion cyclotron frequency.

Considering the perpendicular dispersion relation, we let $n_{||} = 0$ directly and easily obtain

$$k_\perp^2 v_A^2/\Omega_i^2 = y^2, \tag{37}$$

which is a compressional Alfvén wave (CAW).

B. Fully kinetic ions and massless fluid electrons

If we retain only the leading order linear terms for the fully kinetic ion model, then Eq. (5) reduces to

$$\frac{\mathrm{d}w_i}{\mathrm{d}t} = -\frac{1}{f_{\mathrm{i}0}}\delta L f_{\mathrm{i}0}. \tag{38}$$

Using the unperturbed particle orbit integration method, combining Eqs. (2), (3), (8), and (9), and using a uniform Maxwellian distribution function

$$f_{\mathrm{i}0} = n_{\mathrm{i}0}\left(\frac{m_i}{2\pi T_i}\right)^{3/2}\exp\left(-\frac{m_i\left(v_\perp^2 + v_{||}^2\right)}{2T_i}\right),$$

we derive the ion density:

$$\delta n_i = F\left[\frac{lJ_l^2}{k_\perp v_\perp/\Omega_i}v_\perp\right]\delta E_x + F\left[iJ_lJ_l'v_\perp\right]\delta E_y + F\left[J_l^2 v_{||}\right]\delta E_z, \tag{39}$$

and the ion current:

$$\delta \mathbf{j}_\mathbf{i} = \boldsymbol{\sigma} \cdot \delta \mathbf{E}. \tag{40}$$

The conductivity tensor can be written as

$$\boldsymbol{\sigma} = \begin{pmatrix} \sigma_{xx} & \sigma_{xy} & \sigma_{xz} \\ \sigma_{yx} & \sigma_{yy} & \sigma_{yz} \\ \sigma_{zx} & \sigma_{zy} & \sigma_{zz} \end{pmatrix}$$
$$= q_i F \left[\begin{pmatrix} \frac{l^2 J_l^2}{(k_\perp v_\perp/\Omega_i)^2} v_\perp^2 & i\frac{l J_l' J_l}{k_\perp v_\perp/\Omega_i} v_\perp^2 & \frac{l J_l^2}{k_\perp v_\perp/\Omega_i} v_{||} v_\perp \\ -i\frac{l J_l' J_l}{k_\perp v_\perp/\Omega_i} v_\perp^2 & J_l'^2 v_\perp^2 & -i J_l J_l' v_{||} v_\perp \\ \frac{l J_l^2}{k_\perp v_\perp/\Omega_i} v_{||} v_\perp & i J_l J_l' v_{||} v_\perp & J_l^2 v_{||}^2 \end{pmatrix} \right],$$

where $F[\cdots] = i\int\int \frac{2\pi q_i}{T_i} f_{i0} \sum_l \frac{(\cdots)}{\omega - l\Omega_i - k_{||} v_{||}} v_\perp dv_\perp dv_{||}$, J_l is a Bessel function of the first kind of order l, and the argument of J_l is $\xi = k_\perp v_\perp/\Omega_i$.

Now, using Eqs. (22)–(29), (39) and (40), we derive the dispersion relation in which waves propagate perpendicular and parallel to $\mathbf{B_0}$, respectively. In the perpendicular direction, the dispersion relation is

$$\left(\frac{b^2}{0.5\beta_i} + F_1\right)\frac{F_3}{0.5\beta_i} - \left(\frac{b^2}{0.5\beta} + \frac{F_4}{0.5\beta}\right)(1 + F_2) = 0, \tag{41}$$

where

$$b = \frac{k_\perp v_{\mathrm{thi}}}{\Omega_i} = k_\perp \rho_i,$$
$$\beta_i = 2\left(\frac{v_{\mathrm{thi}}}{v_A}\right)^2 = \frac{8\pi n_0 T_i}{{B_0}^2},$$
$$F_1 = \sum_{l=0}^{+\infty} \frac{(2-\delta(l))y^2}{y^2 - l^2} \exp(-b^2)\left(\left(\frac{l^2}{b^2} + 2(b^2 - l)\right) I_l - 2b^2 I_{l+1}\right),$$
$$F_2 = \sum_{l=1}^{+\infty} \frac{2l}{y^2 - l^2} \exp(-b^2)\left(\left(\frac{l^2}{b^2} - l\right) I_l + l I_{l+1}\right),$$
$$\frac{F_3}{0.5\beta_i} = \sum_{l=1}^{+\infty} \frac{4l/\beta_i}{y^2 - l^2} \exp(-b^2) l I_l,$$
$$\frac{F_4}{0.5\beta_i} = \sum_{l=0}^{+\infty} \frac{(4 - 2\delta(l))y^2/\beta_i}{y^2 - l^2} \exp(-b^2)\left((l - b^2) I_l + b^2 I_{l+1}\right),$$

$v_{\mathrm{thi}} = \sqrt{T_i/m_i}$ and $v_A = \sqrt{B_0^2/(4\pi n_0 m_i)}$ are, respectively, the ion thermal speed and Alfvén speed; δ is the Dirac delta function; I_l the first kind modified Bessel function of order l; and the argument of I_l is b^2. If the ion temperature is very low, we have $b \ll 1$, $\beta_i \ll 1$. Then, using the asymptotic formula $I_l(b^2) \approx \frac{1}{l!}\left(\frac{b^2}{2}\right)^l \leqslant b^{2l}$, we retain only the lowest-order terms, and Eq. (41) reduces to

$$\left(y^2 - \frac{b^2}{0.5\beta_i}\right)\frac{b^2}{0.5\beta_i}\frac{1}{1 - y^2} = 0. \tag{42}$$

Then, $y^2 = 2b^2/\beta_i$ is equivalent to $\omega = k_\perp v_A$, which corresponds to a compressional Alfvén wave in fluid theory. We plot the dispersion relation numerically according to Eq. (41), as shown in Fig. 1 for parameter $\beta_i = 0.1$.

The wave descried by Eq. (41) is a generalized electromagnetic IBW (ion Bernstein wave, blue solid line).[32] It becomes a compressional Alfvén wave in the long wavelength limit, and an electrostatic IBW in the short wavelength limit. $\delta B_{||}$, coming from the polarization currents, provides a perpendicular inductive electric field, which causes an electron density perturbation via the $\mathbf{\delta E} \times \mathbf{B_0}$ drift effect, as shown in Poisson equation Eq. (28). The $(1 + F_2)$ term in the dispersion relation comes from $\delta B_{||}$, which is much less important to the dispersion relation in the short wavelength limit. Therefore, $F_3 = 0$ is approximately satisfied, which is very close to the electrostatic IBW dispersion relation. In fact, in the short wavelength limit, the quasi-neutrality condition fails. The electrostatic IBW is recovered exactly when we retain $\nabla_\perp^2 \delta\phi$ in Poisson's equation [Eq. (19)].

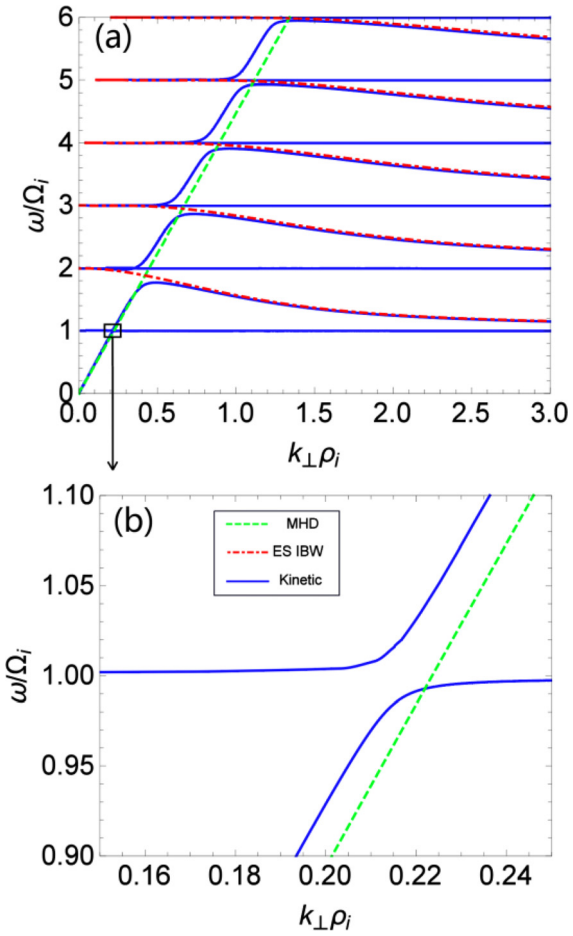

FIG. 1. Perpendicular dispersion relation: (a) over a large wavevector range; (b) zoom in to show the coupling between CAW and the ion cyclotron frequency.

In the parallel direction, assuming $\xi = k_\perp v_\perp/\Omega_i \ll 1$, we have

$$J_n(\xi) = \begin{cases} 1, & n = 0, \\ \pm\xi/2, & n = \pm 1, \\ 0 & others, \end{cases} \quad J_n'(\xi) = \begin{cases} -\xi/2, & n = 0, \\ \pm 1/2, & n = \pm 1, \\ 0 & others. \end{cases}$$

Therefore, the dispersion relation can be written as

$$(Z_3 y - 1)(1 - Z_1) + \left(\frac{1}{\beta_i}\frac{\zeta^2}{y^2} - Z_1\right)\left(\frac{b^2}{0.5\beta_i} - Z_2 y\right) = 0, \quad (43)$$

where

$$Z(x) = \frac{1}{\sqrt{\pi}}\int_{-\infty}^{+\infty}\frac{\exp(-\tau^2)}{\tau - x}\mathrm{d}\tau,$$

$$\zeta = \frac{\sqrt{2}k_{\|}v_{\mathrm{thi}}}{\Omega_i},$$

$$Z_1 = \left(Z\left(\frac{y-1}{\zeta}\right) - Z\left(\frac{y+1}{\zeta}\right)\right)\Big/(2\zeta),$$

$$Z_2 = \left(Z\left(\frac{y-1}{\zeta}\right) + Z\left(\frac{y+1}{\zeta}\right)\right)\Big/(2\zeta),$$

$$Z_3 = \left(Z\left(\frac{y-1}{\zeta}\right) + Z\left(\frac{y+1}{\zeta}\right) - 2Z\left(\frac{y}{\zeta}\right)\right)\Big/(2\zeta),$$

$$Z_4 = \left(\frac{y-1}{\zeta}Z\left(\frac{y-1}{\zeta}\right) + \frac{y+1}{\zeta}Z\left(\frac{y+1}{\zeta}\right) + 2\right)\Big/2.$$

Similarly, at very low ion temperatures, $\zeta \ll 1$, and only the lowest-order terms are retained. Equation (43) now reduces to

$$\left(\frac{b^2}{0.5\beta_i} - \frac{y^2}{1-y^2}\right)\left(\frac{v_A^2}{2v_{\mathrm{thi}}^2} - \frac{y^2}{1-y^2}\right) - y^2\left(\frac{y^2}{1-y^2}\right)^2 = 0, \quad (44)$$

which is exactly the same as Eq. (33) from the fluid theory. The kinetic dispersion relation $b = \frac{5\zeta}{\sqrt{2}}$, $\beta_i = 0.02$ is shown in Fig. 2. Compared with the MHD theory, the kinetic dispersion relation has a lower real frequency and a Landau damping effect.

IV. VERIFICATION OF ICE SIMULATION IN PREPENDICULAR DIRECTION

In this section, we verify the simulation results for the generalized IBW dispersion relation and the excitation of ICE using analytic theory and simple geometry. The model described in Sec. II is implemented in the GTC. The simulations are performed in cylindrical geometry with a uniform magnetic field and uniform equilibrium profile.

We first verify the simulation results of the generalized IBW dispersion relation. We carry out an initial value simulation with parameters $r_0 = 0.3164\,a$, $r_1 = 0.3465\,a$, $\Delta t = 0.0558\Omega_i^{-1}$, and $\omega_{\mathrm{pi}} = 10.05\Omega_i$. Here r_0 is the inner boundary, r_1 is the outer boundary, a is the minor radius, and Δt is the time step. Moreover, we select only the poloidal harmonic m = 0 of the perturbed fields in every time step to mimic slab geometry for verification. In the first simulation, we begin from a random perturbed density and retain modes in the full range of the $k_\perp$ spectrum. The initial random perturbations decay after 18 ion cyclotron periods. The spectral signals are shown in Fig. 3, where the background color represents the mode amplitudes. The analytic dispersion relation is also plotted in Fig. 3 as solid blue lines, which agree very well with the strongest spectral signals from the simulations. In the next simulation, we give an initial perturbed density profile $\frac{\delta n_i}{n_0} = 10^{-5}\sin\left(6 \times 2\pi\frac{r-r_0}{r_1-r_0}\right)$ and filter the field at every time step to allow only a single mode with a $k_\perp = 12\pi/\Delta r$ component. By scanning the value of ρ_i, we obtain the dispersion relation for various $k_\perp\rho_i$, shown in Fig. 3 as blue circles,

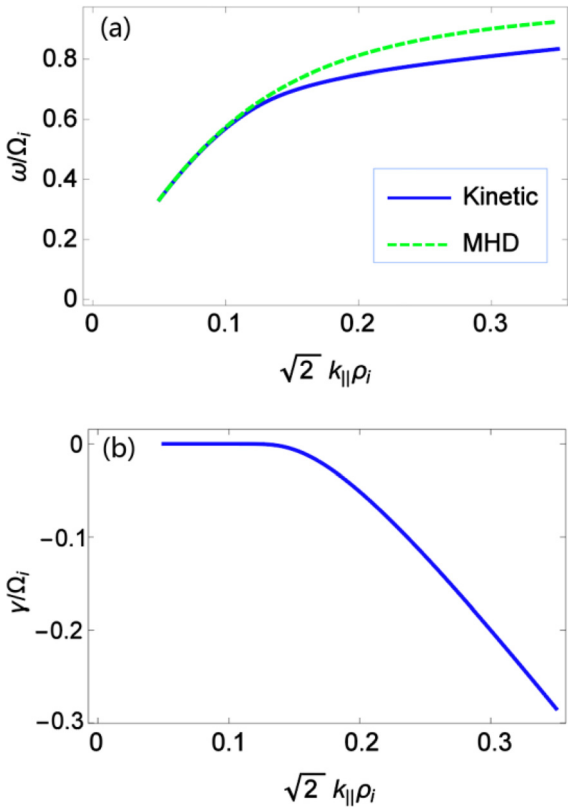

FIG. 2. Parallel dispersion relation from the model with fully kinetic ions and massless fluid electrons: (a) frequency and (b) growth rate as a function of parallel wave vector.

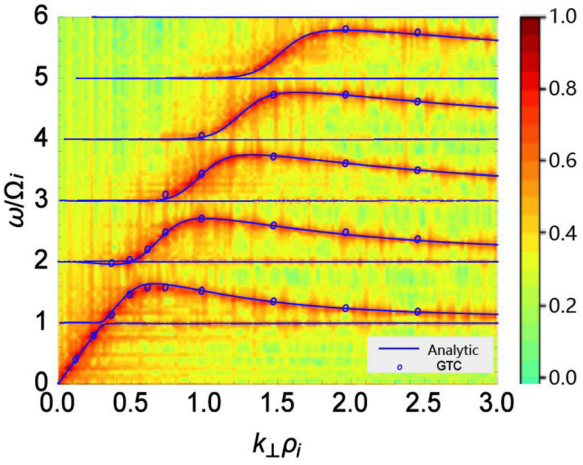

FIG. 3. The dispersion relation. GTC simulation results, keeping all $k_\perp$ modes and only a single $k_\perp$ mode, are represented by the color and blue circles, respectively; solid lines are the analytic kinetic solution.

which agree with the analytic solution. These simulation results provide a solid verification of the physical and numerical models for the ICE simulation in the perpendicular direction. Notably, the signals, especially for high cyclotron harmonics, are very weak when $k_\perp \rho_i$ is very small. It might come from the cyclotron damping effect of bulk ions.

Next, the simulation results for the ICE excited by energetic particles are verified by comparing them with Dendy's analytic theory,[33] which holds the view that ICE arises from a magnetoacoustic cyclotron instability (MCI). The MCI is driven by free energy in the phase space of energetic particles, whose distribution in velocity space exhibits a natural population inversion. The α-particles produced by fusion reaction have, at birth, an isotropic shell distribution in the velocity space. The fast ions produced by the neutral beam injection (NBI) have an anisotropic shell distribution at birth. However, the shell distribution will relax to the slowing-down distribution at the collisional timescale, which is much longer than the MCI excitation time. Therefore, the fast ion distribution with the inverted population that excites the MCI can be somewhere between the shell distribution and slowing-down distribution. An isotropic (spherical) shell distribution has been used in the analytic theory[33] for the MCI excitation. Effects of the spherical shell distribution with a finite thickness and the ring-beam distribution with a perpendicular velocity spread have been shown to affect the excitation and evolution of the MCI in the nonlinear full-f simulations.[21] These physical effects will be further studied in our future nonlinear full-f simulations using the new simulation models described in Sec. II. For the linear δf simulation reported in this paper for the verification of our simulation model, we construct two isotropic distribution functions based on a slowing-down distribution function that has already been implemented in the GTC:

$$F_{f6}(v) = n_f \frac{v^6}{C_6} \frac{H(v_b - v)}{v^3 + v_c^3}$$

and

$$F_{f4}(v) = n_f \frac{v^4}{C_4} \frac{H(v_b - v)}{v^3 + v_c^3},$$

where H is Heaviside function, $v_c = 1.5\sqrt{T_f/m_f}$, $v_b = 2v_c$, $C_6 = \int_0^{v_b} \frac{4\pi v^8}{v^3+v_c^3} dv = \frac{2}{3}\pi(v_b^6 - 2v_b^3 v_c^3 + 2v_c^6 \ln(1 + v_b^3/v_c^3))$, and $C_4 = \int_0^{v_b} \frac{4\pi v^6}{v^3+v_c^3} dv = \pi v_b^4 - 4\pi v_b v_c^3 + \frac{2}{9}\pi v_c^4(\sqrt{3}\pi - 6\sqrt{3}\arctan\left(\frac{v_c - 2v_b}{\sqrt{3}v_c}\right) + 6\ln(v_b + v_c) - 3\ln(v_b^2 - v_b v_c + v_c^2))$. We also use parameters similar to those in the analytic theory: an energetic proton population in deuterium plasmas with parameter values $B_0 = 3.1$ T, $T_i = 1$keV, $T_f = 3$MeV, and $n_0 = 2 \times 10^{13}\text{cm}^{-3}$. Other parameters are $r_0 = 0.3164\,a$, $r_1 = 0.3465\,a$, $a = 0.4242R$, and $(r_1 - r_0)/\rho_i = 1227$. The initial perturbed density profile is $\frac{\delta n_i}{n_0} = 10^{-5}\sin\left(32\pi \frac{r - r_0}{r_1 - r_0}\right)$ and only the $k_\perp \rho_i = 32\pi/(r_1 - r_0) = 0.0819$ component is retained in the simulation. Using these parameters, the linear simulations find the MCI instability.

To ensure that the simulation results are physical, we have verified the conservation of the equilibrium particle kinetic energy as a check for the accuracy of the time integration. More importantly, we have performed numerical convergences for the number of particles per cell and the size of time step size as shown in Fig. 4. The mode $\omega = 4\,\Omega_i = 2\,\Omega_f$ is retained and the F_{f6} distribution function is used

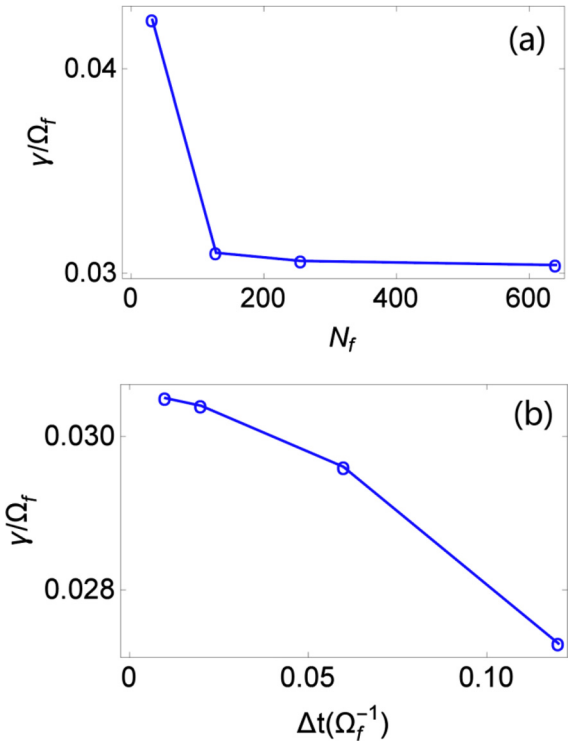

FIG. 4. Numerical convergence studies showing the dependence of the MCI growth rate on: (a) the number of fast ions per radial grid N_f; and (b) the size of the time step Δt.

in these simulations. Considering the converged simulation results, we use 2048 grids in the radial direction, approximately average 6400 thermal ions and 640 fast ions per radial grid, and a time step of $\Delta t = 2.0 \times 10^{-2}\Omega_f^{-1}$ to obtain accurate results in all subsequent simulations. Now we scan the value of n_f/n_0 to obtain the relation between growth rate and concentration of energetic ions, which is shown in Fig. 5. The GTC simulation results of the growth rate for the $\omega = 2\,\Omega_f$

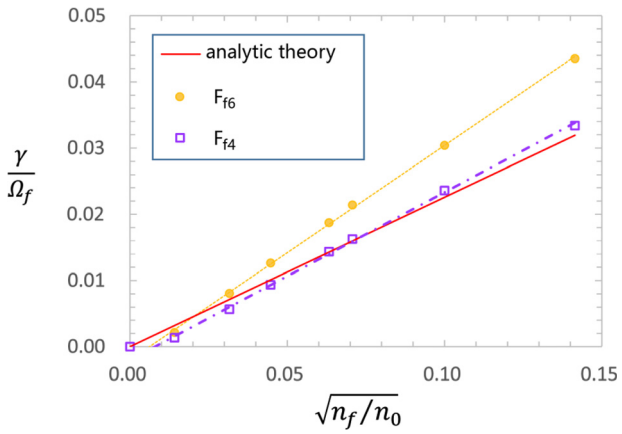

FIG. 5. Dependence of the ICE growth rate on the concentration of energetic ions. The red solid line is from Dendy's analytic theory.[31] Orange points and blue squares are from the GTC simulation using slightly different distribution functions.

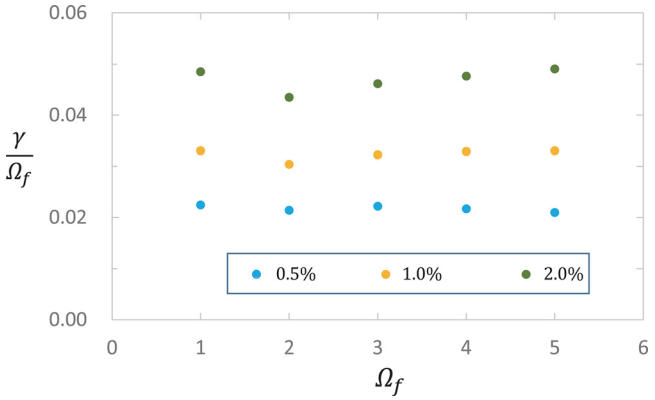

FIG. 6. Linear growth rates of different ICE harmonics for three fast ion concentrations $n_f/n_0 = 0.5\%, 1\%, 2\%$.

mode are plotted as orange points for F_{f6} and blue squares for F_{f4}. Their fitted straight lines (the orange dashed line and the red solid line) show that the growth rate scales linearly as $\sqrt{n_f/n_0}$, which agrees with the analytic theory and other PIC simulations.[14,39] However, there is a difference between the slope in our simulation using F_{f6} and the slope using analytic theory. Our results using F_{f4} have a slope similar to that of the analytic theory. The F_{f6} distribution has a greater inverse population than the F_{f4} distribution and a higher effective temperature than the $T_f = 3$ MeV used in the analytic theory; and therefore, the orange line has a steeper slope. It is worth noting that, when n_f/n_0 is very small ($\sqrt{n_f/n_0} \lesssim 0.01$), the growth rates from the simulations do not follow this linear scaling, implying the existence of bulk ion cyclotron damping effects and confirming previous results.[14] Selecting different $k_\perp \rho_i$ modes in the simulation allows the examination of various resonant frequencies: $\omega = 1, 2, 3, 4, 5\Omega_f$. As shown in Fig. 6, linear growth rates for different harmonics of the ICE are obtained from the fully kinetic simulations using F_{f6} for the three values $n_f/n_0 = 0.5\%, 1\%, 2\%$. The results show that all harmonics have similar growth rates for each concentration of energetic ions.

In future work, we will explore the MCI in relation to the ICE excitation in fusion plasmas in toroidal geometry using nonlinear simulations, comparing the results with other nonlinear 2D simulations.[21,40] We will then validate our model by comparing simulation results with experimental measurement results to study the ICE mode structure, saturation,[9] and amplitude modulation correlated with edge-localized mode (ELM) activity.[41]

V. CONCLUSIONS AND DISCUSSION

A new electromagnetic simulation model, in which ion dynamics is described by a six-dimensional Vlasov equation and electron dynamics is described by a drift kinetic equation or massless fluid equation, was formulated and implemented in the GTC code for simulations of high-frequency waves in the toroidal geometry. Linear dispersion relations of such high-frequency waves in both perpendicular and parallel directions were verified. Using a model with fully kinetic ions and massless fluid electrons, we derived the general IBW dispersion relation in the perpendicular direction and kinetic shear Alfvén wave in the parallel direction, which confirms that our simulation model faithfully preserves the high-frequency waves. Furthermore, the simulation results of the ICE excitation in the cylindrical geometry were verified by comparing them with analytic theory. The simulation results recovered the important scaling of the MCI growth rate with the fast ion concentration.

Furthermore, the nonlinear dynamics of high-frequency waves (ICE, CAE, and GAE waves) will be studied using the new simulation capability.

ACKNOWLEDGMENTS

The authors gratefully acknowledge helpful discussions with J. Bao, A. Kuley, J. Y. Fu, and S. Y. Sun, as well as technical support by the GTC team. This work was supported by the China National Magnetic Confinement Fusion Science Program (Nos. 2017YFE0301300 and 2018YFE0304100) and by the U.S. Department of Energy (DOE) Grant No. DE-SC0021316 and SciDAC ISEP Center. This work used the High-Performance Computing Platform of Peking University and the resources of the Oak Ridge Leadership Computing Facility at Oak Ridge National Laboratory (DOE Contract No. DE-AC05-00OR22725) and the National Energy Research Scientific Computing Center (DOE Contract No. DE-AC02-05CH11231).

AUTHOR DECLARATIONS

Conflict of Interest

The authors have no conflicts to disclose.

Author Contributions

Yangyang Yu: Conceptualization (equal); Data curation (lead); Formal analysis (lead); Investigation (lead); Methodology (lead); Project administration (lead); Software (supporting); Validation (lead); Visualization (lead); Writing – original draft (lead); Writing – review and editing (equal). **Xishuo Wei:** Writing – original draft (supporting); Writing – review and editing (supporting). **Pengfei Liu:** Writing – original draft (supporting); Writing – review and editing (supporting). **Zhihong Lin:** Conceptualization (equal); Formal analysis (supporting); Funding acquisition (lead); Investigation (supporting); Methodology (supporting); Resources (lead); Software (lead); Supervision (lead); Writing – original draft (supporting); Writing – review and editing (equal).

DATA AVAILABILITY

The data that support the findings of this study are available from the corresponding author upon reasonable request.

REFERENCES

[1]N. N. Gorelenkov, E. Fredrickson, E. Belova, and C. Z. Cheng, Nucl. Fusion **43**, 228 (2003).
[2]N. N. Gorelenkov, E. Belova, H. L. Berk, C. Z. Cheng, E. Fredrickson, W. W. Heidbrink, S. Kaye, and G. J. Kramer, Phys. Plasmas **11**, 2586 (2004).
[3]D. Stutman, L. Delgado-Aparicio, N. Gorelenkov, M. Finkenthal, E. Fredrickson, S. Kaye, E. Mazzucato, and K. Tritz, Phys. Rev. Lett. **102**, 115002 (2009).
[4]E. D. Fredrickson, E. V. Belova, D. J. Battaglia, R. E. Bell, N. A. Crocker, D. S. Darrow, A. Diallo, S. P. Gerhardt, N. N. Gorelenkov, B. P. LeBlanc, and M. Podestà, Phys. Rev. Lett. **118**, 265001 (2017).

[5]S. G. Thatipamula, G. S. Yun, J. Leem, H. K. Park, K. W. Kim, T. Akiyama, and S. G. Lee, Plasma Phys. Controlled Fusion **58**, 065003 (2016).
[6]B. Chapman, R. O. Dendy, K. G. McClements, S. C. Chapman, G. S. Yun, S. G. Thatipamula, and M. H. Kim, Nucl. Fusion **57**, 124004 (2017).
[7]L. G. Askinazi, A. A. Belokurov, D. B. Gin, V. A. Kornev, S. V. Lebedev, A. E. Shevelev, A. S. Tukachinsky, and N. A. Zhubr, Nucl. Fusion **58**, 082003 (2018).
[8]R. Ochoukov, V. Bobkov, B. Chapman, R. Dendy, M. Dunne, H. Faugel, M. García-Muñoz, B. Geiger, P. Hennequin, K. G. McClements, D. Moseev, S. Nielsen, J. Rasmussen, P. Schneider, M. Weiland, and J. M. Noterdaeme, Rev. Sci. Instrum. **89**, 10J101 (2018).
[9]K. E. Thome, D. C. Pace, R. I. Pinsker, M. A. Van Zeeland, W. W. Heidbrink, and M. E. Austin, Nucl. Fusion **59**, 086011 (2019).
[10]E. D. Fredrickson, N. N. Gorelenkov, R. E. Bell, A. Diallo, B. P. Leblanc, and M. Podestà, Phys. Plasmas **26**, 032111 (2019).
[11]E. V. Belova, N. N. Gorelenkov, and C. Z. Cheng, Phys. Plasmas **10**, 3240 (2003).
[12]E. V. Belova, N. N. Gorelenkov, E. D. Fredrickson, K. Tritz, and N. A. Crocker, Phys. Rev. Lett. **115**, 015001 (2015).
[13]E. V. Belova, E. D. Fredrickson, J. B. Lestz, and N. A. Crocker, Phys. Plasmas **26**, 092507 (2019).
[14]L. Carbajal, R. O. Dendy, S. C. Chapman, and J. W. S. Cook, Phys. Rev. Lett. **118**, 105001 (2017).
[15]R. O. Dendy, K. G. McClements, C. N. Lashmore-Davies, G. A. Cottrell, R. Majeski, and S. Cauffman, Nucl. Fusion **35**, 1733 (1995).
[16]S. Cauffman, R. Majeski, K. G. McClements, and R. O. Dendy, Nucl. Fusion **35**, 1597 (1995).
[17]G. A. Cottrell, V. P. Bhatnagar, O. D. Costa, R. O. Dendy, J. Jacquinot, K. G. McClements, D. C. McCune, M. F. F. Nave, P. Smeulders, and D. F. H. Start, Nucl. Fusion **33**, 1365 (1993).
[18]K. G. McClements, R. D'Inca, R. O. Dendy, L. Carbajal, S. C. Chapman, J. W. S. Cook, R. W. Harvey, W. W. Heidbrink, and S. D. Pinches, Nucl. Fusion **55**, 043013 (2015).
[19]T. D. Arber, K. Bennett, C. S. Brady, A. Lawrence-Douglas, M. G. Ramsay, N. J. Sircombe, P. Gillies, R. G. Evans, H. Schmitz, A. R. Bell, and C. P. Ridgers, Plasma Phys. Controlled Fusion **57**, 113001 (2015).
[20]S. Markidis, G. Lapenta, and Rizwan-uddin, Math. Comput. Simul. **80**, 1509 (2010).
[21]B. Chapman, R. O. Dendy, S. C. Chapman, K. G. McClements, and R. Ochoukov, Plasma Phys. Controlled Fusion **62**, 095022 (2020).
[22]Y. Lin, X. Wang, Z. Lin, and L. Chen, Plasma Phys. Controlled Fusion **47**, 657 (2005).
[23]J. Müller, S. Simon, U. Motschmann, J. Schüle, K. H. Glassmeier, and G. J. Pringle, Comput. Phys. Commun. **182**, 946 (2011).
[24]G. Y. Fu, W. Park, H. R. Strauss, J. Breslau, J. Chen, S. Jardin, and L. E. Sugiyama, Phys. Plasmas **13**, 052517 (2006).
[25]Z. Lin, T. S. Hahm, W. W. Lee, W. M. Tang, and R. B. White, Science **281**, 1835 (1998).
[26]A. Kuley, Z. X. Wang, Z. Lin, and F. Wessel, Phys. Plasmas **20**, 102515 (2013).
[27]X. S. Wei, Y. Xiao, A. Kuley, and Z. Lin, Phys. Plasmas **22**, 092502 (2015).
[28]J. Bao, Z. Lin, A. Kuley, and Z. X. Lu, Plasma Phys. Controlled Fusion **56**, 095020 (2014).
[29]A. Kuley, Z. Lin, J. Bao, X. S. Wei, Y. Xiao, W. Zhang, G. Y. Sun, and N. J. Fisch, Phys. Plasmas **22**, 102515 (2015).
[30]J. Lin, W. Zhang, P. Liu, Z. Lin, C. Dong, J. Cao, and D. Li, Nucl. Fusion **58**, 016024 (2018).
[31]J. Bao, Z. Lin, A. Kuley, and Z. X. Wang, Nucl. Fusion **56**, 066007 (2016).
[32]R. W. Fredricks, J. Plasma Phys. **2**, 365 (1968).
[33]R. O. Dendy, C. N. Lashmore-Davies, and K. F. Kam, Phys. Fluids B **4**, 3996 (1992).
[34]Y. Xiao, I. Holod, Z. Wang, Z. Lin, and T. Zhang, Phys. Plasmas **22**, 022516 (2015).
[35]J. Bao, Z. Lin, A. Kuley, and Z. X. Wang, Phys. Plasmas **23**, 062501 (2016).
[36]Z. Lin, S. Ethier, T. S. Hahm, and W. M. Tang, Phys. Rev. Lett. **88**, 195004 (2002).
[37]H. Feng, W. Zhang, Z. Lin, X. Zhufu, J. Xu, J. Cao, and D. Li, Commun. Comput. Phys. **24**, 655 (2018).
[38]T. H. Stix, *Waves in Plasmas* (AIP, New York, 1992).
[39]B. C. G. Reman, R. O. Dendy, T. Akiyama, S. C. Chapman, J. W. S. Cook, H. Igami, S. Inagaki, K. Saito, and G. S. Yun, Nucl. Fusion **59**, 096013 (2019).
[40]L. Carbajal and F. A. Calderón, Phys. Plasmas **28**, 014505 (2021).
[41]N. A. Crocker, S. X. Tang, K. E. Thome, J. B. Lestz, E. V. Belova, A. Zalzali, R. O. Dendy, W. A. Peebles, K. K. Barada, R. Hong, T. L. Rhodes, G. Wang, L. Zeng, T. A. Carter, G. H. Degrandchamp, W. W. Heidbrink, and R. I. Pinsker, Nucl. Fusion **62**, 026023 (2022).